J Solid State Electrochem (2007) 11:1145–1156
DOI 10.1007/s10008-006-0252-6

ORIGINAL PAPER

Properties of nanocrystalline electrodeposited CoFeP alloy with low phosphorus content

Egwu E. Kalu

Received: 18 August 2006 / Revised: 1 November 2006 / Accepted: 10 November 2006 / Published online: 10 January 2007

Abstract CoFe and low phosphorus containing (<4 at.%) CoFeP alloy films were electrodeposited from NaH_2PO_2 containing solutions at pH 4 on copper substrates under galvanostatic conditions. At the low phosphorus composition, nanocrystalline CoFeP alloy films are formed. The structure, composition and morphology of the thin films were studied using X-ray diffraction, energy dispersive spectroscopy and atomic force microscopy. The magnetic properties of the film were studied using superconducting quantum interference device magnetometer. The thin film performance features were explained on the basis of microstructural features developed during deposition. Whereas the electrodeposited CoFe alloy thin film exhibited mixed hcp and fcc phase structure in the absence of phosphorus, the low phosphorus containing thin film exhibited an increasing mixed bcc and hcp phase structure as its phosphorus content increases, showing modification in the grain size morphology and magnetic properties. In addition to applied current, the amount of P co-deposited in CoFeP alloy depends on the concentration of NaH_2PO_2 source in the bath. Qualitative analysis of the Tafel slope of CoFe and CoFeP deposition suggests that the presence of P in the CoFe deposit does not affect the mechanism of anomalous deposition of Co and Fe, thereby suggesting that CoFeP deposition is anomalous.

Keywords Electrodeposition · CoFeP · Magnetic · Alloys · Nanocrystalline · Coercivity · Anomalous · Co-deposition · CoFe

E. E. Kalu (✉)
Department of Chemical and Biomedical Engineering,
FAMU-FSU College of Engineering,
Tallahassee, FL 32310, USA
e-mail: ekalu@eng.fsu.edu

Introduction

The use of nanostructured films makes possible the development of new kinds of electronic, optoelectronic and magnetic microelectromechanical systems (MEMS) devices. Examples of such nanostructured thin films include permalloy that may be used for micromagnetic sensor (read/write head), microactuators and frictionless microgears. The explosion in information generation, exchange and storage has necessitated the need for higher recording density greater than the current 100 Gbits/in^2. Before the recent rise in demand for large information storage and exchange, permalloy was satisfactorily used for thin film heads because of its high saturation magnetic induction, high permeability and low coercivity. However, with a steady increase in both the magnetic recording density requirement (>100 Gbits/in^2) and coercivity (H_c) of recording media, it has become apparent that the saturation magnetic induction (B_s) of permalloy film may not provide enough magnetic field intensity to write transitions in high coercive media. Therefore, ferromagnetic thin film that can be potentially applied as micromagnetic sensor reading heads and capable of generating stronger magnetic field than permalloy is needed. Similarly for microactuators application, Co and its alloys are known to have advantage over permalloy. CoFe alloy was one of the ferromagnetic thin films earlier identified as a possible replacement for permalloy [1, 2]. Although CoFe alloy has high magnetic saturation (M_s), it has poor corrosion resistance and low electrical resistivity. Several approaches have been utilized to ameliorate the shortcomings of CoFe. These methods include the addition of a third and fourth elements, the variation in the composition of Fe and amount of bcc phase in the alloy [3]. Variation of Fe composition and the amount of bcc phase in the nanocomposite CoFe alloy can be used

to control its saturation induction (B_s). The addition of a third element in CoFe alloy can improve its electrical, magnetic and corrosion properties. Chang et al. [4] developed CoFeCu with soft magnetic properties, whereas CoFeCr alloy with improved corrosion resistance was reported in [5, 6]. Takai et al. [7] reported the preparation of soft magnetic alloys based on amorphous CoFeP. Hironaka and Uedaira [8] studied amorphous CoFeP and CoFeSnP alloys electroplated by pulse-plating technique. They found that the addition of P (≥11%) into CoFe alloy reduces its saturation magnetization substantially. The addition of Sn (of about 7 wt.%) improves the corrosion resistance of the CoFeP alloys. Gigandet et al. [9] studied the influence of Cu addition on the corrosion properties of CoFe and found that copper improves the passivation ability of the CoFeCu alloys up to 2.7%. Kim et al. [10] conducted systematic studies of NiCo and CoFe thin films, relating their magnetic properties with film composition, grain size and crystal structure. In an earlier report, the influence of phosphorus composition on the magnetic and structural properties of CoFeP thin films was discussed [11].

The functional properties of CoFeP alloy depend on its composition. At P≥11.0 wt.%, CoFeP alloy is amorphous [7] with characteristic properties. This suggests that with P<11.0 wt.%, it is possible for the CoFeP alloy to exhibit performance characteristics different from the amorphous thin film. The film composition is determined by the plating variables. Hence, the development, control and manufacture of CoFeP thin film alloys capable of meeting magnetic recording and MEMS needs of the future will benefit from an understanding of the relationship between the plating variables and the deposited film properties. Bertazzoli and Pletcher [12] showed that the composition of the CoFe alloy is mainly determined by the ratio of Fe(II)/Co(II) in solution. Lallemand et al. [13] examined the influence of organic additives on the kinetics and structure of CoFe deposition.

The literature on CoFeP alloy thin film electrodeposition documents mostly amorphous alloy films of high P content (≥11%) whose magnetic properties are not measured with a superconducting quantum interference device (SQUID) magnetometer. There has not been a thorough examination of magnetic properties of CoFeP at low phosphorus content as has been done for nickel-containing alloys [10, 14, 15]. Rather, in most discussions of CoFeP alloy properties, the extrapolation of the behavior of CoNiP to CoFeP is often assumed and adopted. Although justifiable for the amorphous phase (P≥11 at.%), the extrapolation may not necessarily be true for the microcrystalline phase judging from the behavior of the binary alloys CoP, NiP and FeP when they transition from microcrystalline to amorphous phase [16]. Myung et al. [15] observed that for low phosphorus concentrations in the bath and the alloy, nickel-containing alloys of CoP only show increase in coercivity with increasing amount of P in the alloy only. This behavior for coercivity occurs for low P concentrations in the bath until the coercivity reaches a maximum, whereupon it decreases with increasing P content. Fundamental interest in understanding the relation between the magnetic and structural properties of the binary alloys FeP and CoP [17–20] exists. Extension of interest in the binary alloys to understanding the CoFeP system is a natural evolution of knowledge. Magnetic properties being extrinsic properties and thus influenced only by film composition suggest that manipulation of factors that influence film composition can be utilized as a tool in fabricating thin films of requisite magnetic properties. The factors that can affect these magnetic properties include grain size, stress, crystal structure, surface roughness and film thickness.

In this work, we present a study of the properties of a low phosphorus containing microcrystalline CoFeP alloy thin film prepared under diffusion- and migration-limited conditions at a constant pH 4 and magnetic measurement conducted with SQUID magnetometer. Some special magnetic sensor applications and MEMS require CoFeP thin film of very low phosphorus content. Unlike previous works that examined the electrodeposition of amorphous CoFeP thin film, the present work examines only microcrystalline CoFeP alloy composition (P≤4%). In addition, we qualitatively examine the anomalous mechanism of CoFe deposition in the presence of co-deposited phosphorus.

Materials and methods

Water from a Milli-Q water purification system and analytical grade chemicals (Fisher Chemicals) were used in the preparation of electrodeposition solutions. A freshly prepared stock solution of 0.5 M boric acid and 0.5 M sodium sulfate was used in the preparation of the plating solutions. Solutions were adjusted to pH 4 and deoxygenated with N_2 before each experiment. The experiments were conducted at room temperature with nitrogen passing over the solution during the experimental runs. The solution was not stirred, and thus, mass transfer was purely by diffusion and migration. All the solutions contained 0.5 or 0.1 M $CoCl_2 \cdot 6H_2O$, 0.1 M $FeSO_4 \cdot 7H_2O$ and varying amounts of sodium hypophosphite as the source of phosphorus. To achieve thin films of low phosphorus content, sodium hypophosphite was used as the source for phosphorus. Unlike phosphate ion, hypophosphite ions provided low phosphorus content under the experimental conditions used in this work. Moreover, unlike the reduction in hypophosphite

that involves transfer of one electron, the reduction in phosphite and phosphate ions involves the transfer of multiple (three and five, respectively) electrons. Although a known reducing agent for electroless deposition, hypophosphite ion was not used as a reducing agent under the plating conditions (pH and temperature) used in this work. All metallic reductions occurred through electrochemical route, as no deposition was observed in the absence of applied current.

Cyclic voltammetric studies were carried out in a three-electrode cell. The working electrode was a stationary glassy carbon disc (0.071 cm^2) with a platinum wire counter electrode. Ag/AgCl reference electrode was used. Cyclic voltammograms were recorded for solutions of Co (II), Fe(II) and their mixtures with sodium hypophosphite at a potential scan rate of 20 mV/s. The scan rate of 20 mV/s was chosen because it yielded the most reproducible results for all the conditions examined.

For the electrodeposition experiments, copper plates were used. After cleaning with acetone, the copper surface was etched in 20 vol.% (v/o) HNO_3 solution, weighed and insulated with Scotch tape to define an effective surface area for plating. Galvanostatic deposition was carried out with a Solartron potentiostat/galvanostat (Model 1270) at current densities of 5–25 mA/cm^2 and for periods of 180–300 s. The experiments were repeated three times at each current density, and some of the results presented depict average of three experiments conducted at the same operating conditions. The thickness of the deposit was estimated gravimetrically.

To obtain detailed information about the surface morphology of the films such as grain size structure and roughness of the alloy deposit, the samples were analyzed using a contact/tapping mode atomic force microscopy (AFM; Digital Instruments, Model: Dimension 3000). All the samples were studied in air, and the surface of the alloy deposit was scanned with etched silicon tapping probes, whereas the alloy composition was determined by scanning electron microscopy with energy dispersive spectroscopy (EDS) analyses using the scanning electron microscope (JEOL-JSM 840A). The EDS analyses were performed operating at 15 kV. For the crystal structure and grain size, X-ray diffraction (XRD) studies using Co K_α radiation (λ =1.5406 Å) were carried out using Philip's X-ray diffractometer (Philip's, X Pert) at an operating voltage of 45 kV and current of 40 mA. The XRD was scanned from 2θ position 10° to 2θ position 90° with a step-size of 0.02° and a time per step of 0.5 s. The magnetic measurements of the thin films were carried out at 300 K using Quantum Design (MPMS) SQUID magnetometer in fields up to 5 T. The magnetometer has a sensitivity of 10^{-7} emu, and the external field H was applied parallel to the deposited film plane.

Results and discussion

Electrochemical bath characterization

The cyclic voltammograms on glassy carbon electrode of solutions containing Co(II), Fe(II) and their mixtures with phosphorus are shown in Fig. 1. Figure 1a shows the voltammograms for two different solutions. One solution contains 0.5 M cobalt (II) and the other contains 0.1 M iron (II). For the cobalt solution, the cathodic current increased rapidly after −1.1 V (vs Ag/AgCl), towards a peak value. After passing through the cathodic peak, the cathodic current decreased smoothly to zero after which an anodic current is initiated. This anodic current peaked at −0.62 V. Except for a slight shoulder towards the tail end of the anodic *i–E* curve, no multiple anodic stripping peaks was observed for the experimental conditions contrary to the report in [21]. A similar trend is observed for iron solution, except that the cathodic current increased rapidly at −1.3 V, and the anodic peak current occurred at a more negative potential (−0.9 V) than the cobalt. The cyclic voltammetry (CV) shows that formation of iron requires a more negative potential than for cobalt. This is expected, as cobalt is noble to iron. On the other hand, when both ions are present (Fig. 1b), we observe a single anodic stripping peak at −0.73 V. A single anodic peak for the alloy suggests either the dissolution of the binary alloy occurs simultaneously, or the dissolution of Fe and Co in the binary alloy proceeds very close to each other. The CVs of the individual metals and their alloy (Fig. 1a,b) follow the same general trend. Because the shape of the *i–E* characteristic reflects the kinetics of the metal/metal ion couple, qualitatively, it suggests then that the mechanism of the major electrode reactions in the alloy deposition could be similar as in the individual metal deposition with little or no competing hydrogen evolution. This is in agreement with the widely accepted multi-step reaction-plating model of Bockris [22] for the electrodeposition of all iron-group metals. It is also observed that the addition of Fe^{2+} to cobalt solution causes a negative shift in the deposition potential of cobalt. This means that the addition of Fe^{2+} inhibits Co deposition and consequently changes the mechanism of Co deposition [23–26]. This is characteristic of anomalous co-deposition [23], although the degree of anomalous behavior here is lower than that observed in CoNi co-deposition. Based on our results and data from reference [12], it qualitatively suggests an anomalous co-deposition mechanism for CoFe in which the mechanism for the more noble species changes in the presence of the less noble species [23]. A feature of anomalous behavior exhibited here is that ratio of Fe/Co in the alloy is higher than in the solution (see below). As reported in reference [12], the Fe/Co ratio in the alloy is much higher at lower Fe^{2+} concentration in the solution. Similar to the models of Matlosz [26] and Zech et al. [24],

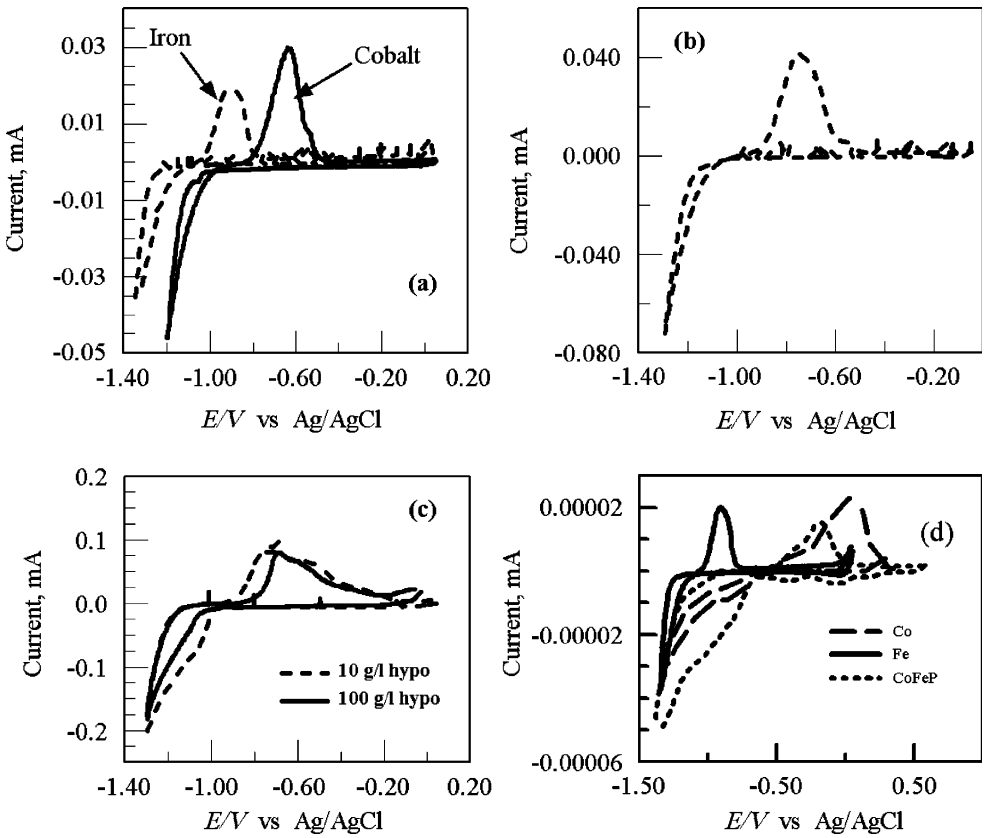

Fig. 1 CV on glassy carbon electrode of solutions containing Co(II), Fe(II) and their mixtures with phosphorus. All solutions were in 0.5 M sodium sulfate and 0.5 M boric acid with pH adjusted to four. Scan rate=20 mV/s. **a** 0.5 M Co(II) only and 0.1 M Fe(II) only, **b** 0.5 M Co(II)+0.1 M Fe(II), **c** 0.5 M Co(II)+0.1 M Fe(II)+P as sodium hypophosphite, **d** 0.1 M Co(II) only, 0.1 M Fe (II) only and 0.1 M Co(II)+ 0.1 M Fe(II)+P as 10 g/l sodium hypophosphite

we postulate that in the absence of iron, cobalt follows the hydrated ion mechanism (three steps) involving adsorption and desorption:

$$Co^{2+} + 2H_2O \Leftrightarrow CoOH^+ + H_3O^+ \quad (1)$$

$$CoOH^+ + M + e \Leftrightarrow Co(OH)\ldots M_{ads} \quad (2)$$

$$Co(OH)\ldots M_{ads} + e \Leftrightarrow Co + OH^- + M \quad (3)$$

where $Co(OH)\cdots M_{ads}$ refers to adsorbed cobalt hydroxide on site M and step 3 is the rate determining step. However, in the presence of iron [though $Co(OH)^+$ may be formed], cobalt reacts through the divalent species (see Eq. 4), which does not adsorb on the electrode. This argument is unlike the approach used in models of references [24] and [26]:

$$Co^{2+} + 2e \Leftrightarrow Co \quad (4)$$

$$Fe(OH)^+ + M + e \Leftrightarrow Fe(OH)\ldots M_{ads} \quad (5)$$

$$Fe(OH)\ldots M_{ads} + e \Leftrightarrow Fe + OH^- + M \quad (6)$$

Here, Co^{2+} competes for vacant sites with the hydrated iron, $[Fe(OH)^+]$ whose mechanism is not affected by the presence of cobalt. The rate-determining step is then step 4. Qualitatively, this line of argument is supported by the data in [12] in which a Tafel slope of 120 mV (α=0.5, n=1) is obtained for cobalt alone and a slope of 60 mV (α=0.5, n= 2) when iron is present. The results in reference [12], like present analysis, were obtained with glassy carbon electrodes for which hydrogen has high evolution overpotential. Further, the postulated model of consecutive reaction mechanism and blocking of surface by adsorbed species is similar to those proposed by a number of authors [23–26].

The existence of hydrated cobalt and iron species in aqueous solution of 0.5 M sodium sulfate and 0.5 M boric acid adjusted to pH 4 (used in this work) is supported by a comparison of the standard potentials of both Co^{2+} and Fe^{2+} found in the literature vs the values obtained in the medium of present work [27]. The calculated standard potentials of −0.49 and −0.62 V vs Ag/AgCl for Co/Co^{2+} (0.5 M) and Fe/Fe^{2+} (0.5 M), respectively, differ from the values found for the solutions of the single metal ions in this work at −0.53 V for Co/Co^{2+} and −0.99 V for Fe/Fe^{2+}. It is clear from these values that both Co^{2+} and Fe^{2+} are complexed in the medium of the experiments and justifies the postulation of the existence of hydrated ions. The speciation of cobalt (or iron) is primarily regulated by pH and the concentration of chelating agents. At neutral or slightly above neutral pH, Co exists as free Co^{2+} sulfate. At very low pH, cobalt is oxidized to the trivalent cobalt and is

usually associated with iron and primarily taken into solution.

In addition to the above, the primary question of interest should be: "Is CoFeP deposition anomalous?" That is, does the presence of P and its co-deposition with CoFe to form CoFeP alloy change the anomalous mechanism of CoFe deposition? This question has not been examined in the literature. Probably, the assumption is that the presence of P does not alter the mechanism of CoFe deposition. For the present work, the effect of phosphorus on the mechanism of the CoFeP alloy deposition is qualitatively examined by evaluating the linear Tafel slope ($2.303RT/\alpha n_a F$). Potential range chosen occurs during the rising portion of i vs E deposition curve. In this potential range, metal deposition is actively taking place, and the slopes correspond to all the electrochemical processes occurring on the surface of the electrode. The log i vs E plots show linear regions with negative slopes ranging from 52 to 60 mV/decade for the Co deposition to a range of 80 to 120 mV/decade for the binary deposition in presence of phosphorus ions. Although the Tafel slope for CoFe deposition obtained in this work is greater than 60, however. contrary to the results in [12], the Tafel slope was lower than 120 mV/decade. The average Tafel slope values obtained are summarized in Table 1. The hypothesis of a mechanism change when Co and Fe are co-deposited is supported by the results in Table 1. In support of anomalous behavior, Table 1 also shows that the ratio of Fe/Co in the alloy is higher than in the solution even when P was present. Further, one would have expected the inclusion of phosphorus (co-deposition) with CoFe alloy to affect the alloy deposition mechanism; however, Table 1 results suggest that the presence of phosphorus appears not to affect the mechanism of CoFe alloy electrodeposition. The value of the transfer coefficient corresponding to the slopes calculated for Co (52 mV/decade) and Fe (60 mV/decade) is 0.57 and 0.5, respectively. For the CoFe containing species (including the phosphorus containing ones), the transfer coefficient ranges from 0.6 to 0.88 suggesting multiple-electron transfer process.

Table 1 Tafel slopes obtained for different baths and Fe/Co ratio in support of a mechanism change when Co and Fe are co-deposited

Species	Tafel slope $=-\frac{2.303RT}{\alpha_c nF}$	Fe/Co ratio in alloy
Co	52	–
Fe	60	–
CoFe	67	0.239
CoFeP (1 g/l hypo)	100	0.300
CoFeP (100 g/l hypo)	87	0.303
Solution	–	0.190[a]

[a] Fe/Co ratio in the electrolyte bath

Figure 1c shows the voltammograms obtained when phosphorus is included in the mixed solution of Co(II) and Fe(II). The key points are that the onset potential for CoFeP deposition on glassy carbon electrode is around −1.1 V, and the areas under the cathodic and anodic peaks decreased with increase in hypophosphite ion concentration. The onset potential for deposition of the CoFeP alloy is similar to the value obtained in the absence of phosphorus, suggesting that the presence of phosphorus does not change the reaction mechanism associated with binary alloy. The area difference with increase in hypophosphite concentration suggests that the phosphorus may be adsorbed on the electrode surface before being co-deposited. The anodic peak current is slightly more noble in the solution containing the higher hypophosphite concentration (*cf.* −0.7 and −0.66 V).

Although the overall shape of the i–E characteristic curve for CoFeP is similar to that obtained for the single metal ions, Fig. 1d suggests the presence of competing cathodic process during the scan in the negative direction. Unlike the single metal voltammograms that follow the zero current potential before the initiation of metal deposition, some cathodic currents existed before metal deposition in the presence of P. The cathodic current could have been double-layer charging (non-faradaic current) or faradaic current due to unknown competing reactions. The cause or nature of the small cathodic current was not pursued in this work, as it did not appear to have affected the mechanism of reactions of interest.

Microstructural studies

The AFM 3D images of the surface of galvanostatically (10 mA cm^{-2}) deposited thin films of CoFe and CoFeP alloys are depicted in Fig. 2. The figures consist of aggregates of grains of different sizes randomly disseminated over the sample surfaces. However, the surface layers of the three images differ in some respects. Figure 2a shows that the CoFe sample exhibits aggregates of rounded top. Relative to Fig. 2b,c, the size distributions of the aggregates in Fig. 2a are more uniformly distributed. Unlike Fig. 2a, the aggregate grains of Fig. 2b are distributed less uniformly (that is, the size differences between the large and small grains of sample are more pronounced), and these aggregates exhibit a needle-like (columnar) appearance. Although grains of Fig. 2c exhibit sharp top needle-like aggregates, these needle-like aggregates are sharper and thinner than those found in Fig. 2b. Also, Fig. 2c grains are less uniform in terms of size distribution. The three samples in Fig. 2 differ by the amount of phosphorus in their composition. Whereas the bath of Fig. 2a did not contain any phosphorus, the bath from which sample 2b was obtained contained 1 g/l hypophosphite (<1.3 at.% P),

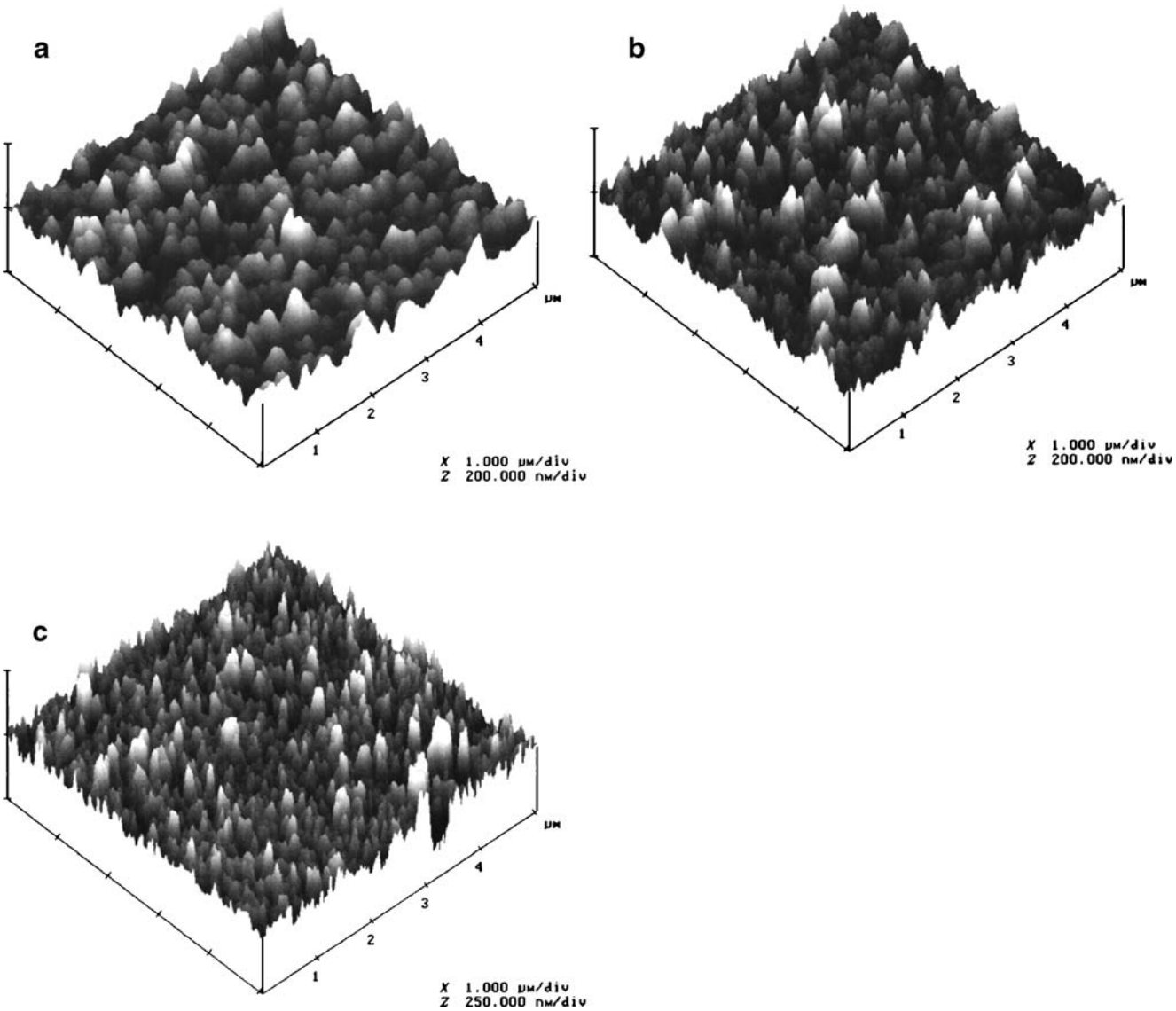

Fig. 2 AFM 3-D images of CoFeP alloy electrodeposited on a copper substrate at 10 mA/cm^2. Conditions are: **a** 0.5 M Co(II)+0.1 M Fe(II), **b** 0.5 M Co(II)+0.1 M Fe(II)+1 g/l hypophosphite and **c** 0.5 M Co(II)+0.1 M Fe (II)+10 g/l hypophosphite

while the bath for sample 2c had 10 g/l hypophosphite (1.8 at.% P). The results suggest that addition of phosphorus to CoFe modulates the microstructural properties (structure and morphology) of the deposit including change in the aspect ratio of the aggregates and uniformity of deposit coverage.

From practical applications point of view, for example, security documents embedded with thin magnetic film, the roughness of the final films is very important. The root mean square (RMS) roughness (nanometer) values obtained for the surfaces using AFM indicate that the addition of phosphorus changes the surface roughness of the deposit. Increasing phosphorus content results in smoother surface morphology. The roughness is also dependent on the total charge passed as expected. Figure 3 illustrates the relationship between the total coulombs passed and roughness of the CoFe and CoFeP thin films. For both alloys, the roughness decreases with increase in total charge passed. On passing same quantity of deposition charge, Fig. 3 suggests that the roughness of electrodeposited CoFeP thin film will be lower than that of CoFe deposit. In the work of Park et al. [14], the morphological changes of CoNiP electrodeposit was controlled by the P content of the deposit. The morphology of the deposit becomes smoother with increasing P content similar to the observation made with increasing P in the present work. Similarly, as in [14], the pH and applied current density play significant role in the electrolytic deposition.

An examination of the AFM 2D deposits (Fig. 4) was used for further comparison. Unlike the samples that contain

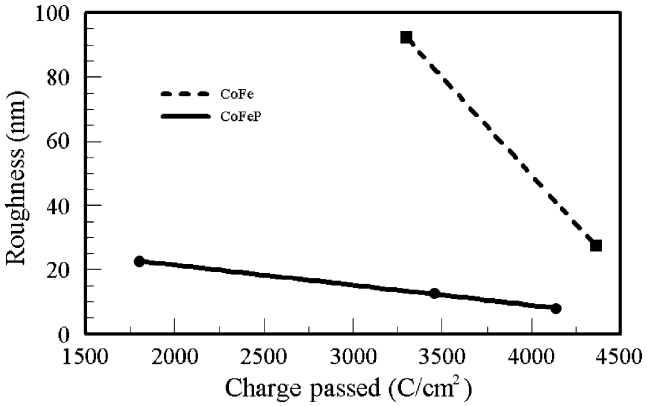

Fig. 3 RMS roughness of thin film deposit as a function of total charge passed

phosphorus, examination of the (AFM picture) morphology of the deposits that contain only cobalt and iron show (Fig. 4a) that the films consist CoFe nanocrystallites. A cross-section of several samples shows particles of varying sizes. The average particle size estimated (using AFM pictures) for the film containing only Co and Fe was 16 nm. The grains of CoFe only deposits are also segregated in their respective coalesced groups. This is quite unlike samples that contain phosphorus in addition to Fe and Co. The grains of CoFeP samples with low P content (Fig. 4b) are slightly elongated grains that coalesce together (aggregate) into larger grains. The average size for these elongated and coalesced grains appear slightly greater than do those of non-phosphorus containing samples. With increase in P content, the elongated feature observed for low P samples seems to be further developed into a honeycomb appearance (Fig. 4c). The average size of the grains for the samples with higher amount of P is even more than the low P containing samples. Some of the elongated grains of the high P samples reached a length of 189 nm. The results suggest that the presence of phosphorus in the CoFe alloy changes the average grain size and elongates it too. It is thus apparent then that with increase in P, a level of P can be reached at which the alloy deposit will become amorphous. We did not determine that window of P composition between complete amorphous and crystallinity for CoFe. However, at P content of less than 4 at.%, the samples still show some crystallinity. The addition of low amounts of phosphorus to CoFe films produces nanocrystalline films with a modified crystal structure and morphology. The modified structure affects the energy barriers required for the magnetic alignment of the CoFe grains; thus, the performance properties of such CoFeP thin films differ both from those of crystalline CoFe bimetallic alloy and the totally amorphous CoFeP alloy. This is important for the sensor application envisaged for the present thin film samples.

The crystal structure and the grain size of the thin films were characterized using XRD for the crystalline phases. As revealed by the XRD analysis (Fig. 5), the as-deposited $Co_{1-x}Fe_x$ films from hypo-free solution exhibited a mixed structure of fcc (111), bcc (110) or hcp (002) and fcc (200) planes. The data is consistent with equilibrium phase diagram predictions for the binary $Co_{1-x}Fe_x$ system in which $0.1 \leq x \leq 0.25$ and the thermodynamic stability indicates a mixture of disordered bcc phase and fcc structure [28]. For thin films of CoFe deposited by molecular beam epitaxy on a number of different samples, Wojcik et al. [20] observed a shift in the stability limits of the bcc structure. The result in [20] shows that for Fe concentrations larger than $x=0.11$, a sample consistent with bcc lattice is obtained, whereas lower Fe concentration results in an abrupt switch to fcc phase. This suggests that the stability limits of bcc structure are shifted from $x=0.25$ (as predicted in reference [28] in case of bulk alloys) to $x=0.11$ for the epitaxial alloys. For the present work, the composition of the $Co_{1-x}Fe_x$ thin film is such that $0.19 \leq x \leq 0.23$, and thus, all the samples fall into the predicted thermodynamic equilibrium region. In the absence of hypo, Fig. 5a reveals a predominant fcc (111), and fcc (220) phases with low bcc peaks spread out in the matrix. However, with hypophosphite present in the bath (Fig. 5b,c), the fcc peaks at (111) and (220) planes are dramatically reduced, whereas the bcc (110) or hcp (002) peaks at $2\theta=45.19$, and bcc (211) at $2\theta=83.57$ increased in size. As Fe contents of the alloy samples were ~19 at.% (Fig. 5a), 23 at.% (Fig. 5b) and 23 at.% (Fig. 5c), the changes in preferred orientation can possibly be attributed to the presence of phosphorus, which was 0, 1.6 and 3.3 at.%, respectively, for Fig. 5a,b and c. Thus, the presence of P in the deposit changes the preferred orientation of the CoFe alloy deposit from fcc (111) plane to hcp (002) or bcc (110) plane. This is consistent with the result obtained by Park et al. [14] for CoNiP thin film electrodeposited from a hypophosphite bath. As observed by Kim et al. [10], it is difficult to index the peak at ~45.19° [either hcp (002) or bcc (110)], although one can argue for the disordered bcc phase [bcc (110)] based on the bulk equilibrium phase diagram of the binary CoFe system as in reference [28]. Using the XRD patterns, the grain size of the CoFe and CoFeP deposits with preferred hcp (002) planes were estimated using Scherer formula. The grain size estimates were ~12 nm (CoFe only), 12.3 nm (CoFeP, 1% hypo) and 16.3 nm (CoFeP, 10% hypo). The trend is in agreement with the estimate obtained using AFM data.

Although the size and sharpness of the diffraction peaks of the CoFe containing phosphorus alloy deposits (CoFeP) differ from those of CoFe only alloy (no phosphorus), the samples remain crystalline at the low phosphorus content used in this work. For the CoFe only alloy deposit, the XRD results in Fig. 5a indicate a texture with fcc structure for as-deposited CoFe alloy. Assuming a solid solution

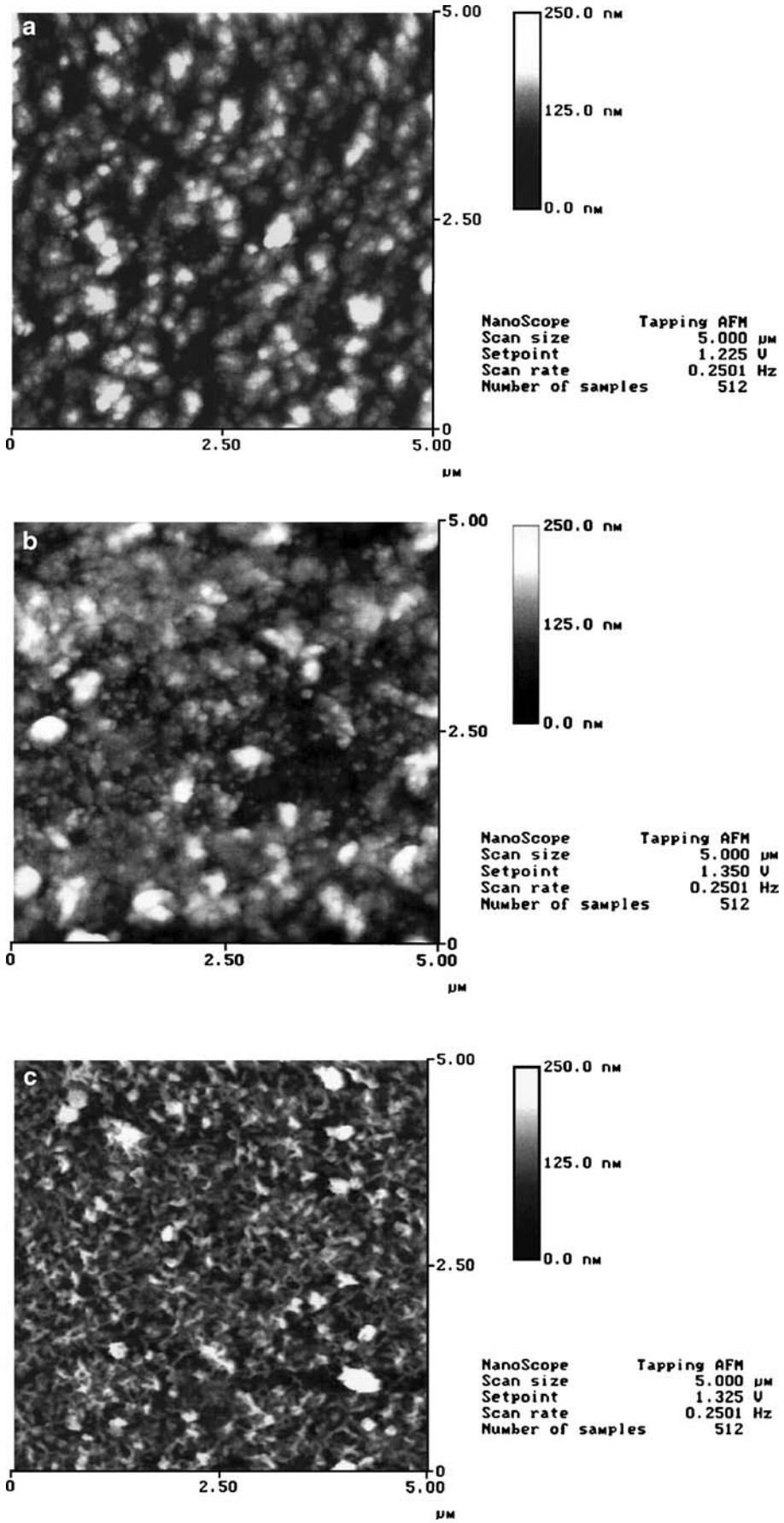

Fig. 4 AFM 2-D images of CoFeP alloy electrodeposited on a copper substrate at 13 mA/cm^2. Conditions are: **a** 0.5 M Co (II)+0.1 M Fe(II), **b** 0.5 M Co (II)+0.1 M Fe(II)+1 g/l hypophosphite and **c** 0.5 M Co(II)+ 0.1 M Fe (II)+10 g/l hypophosphite

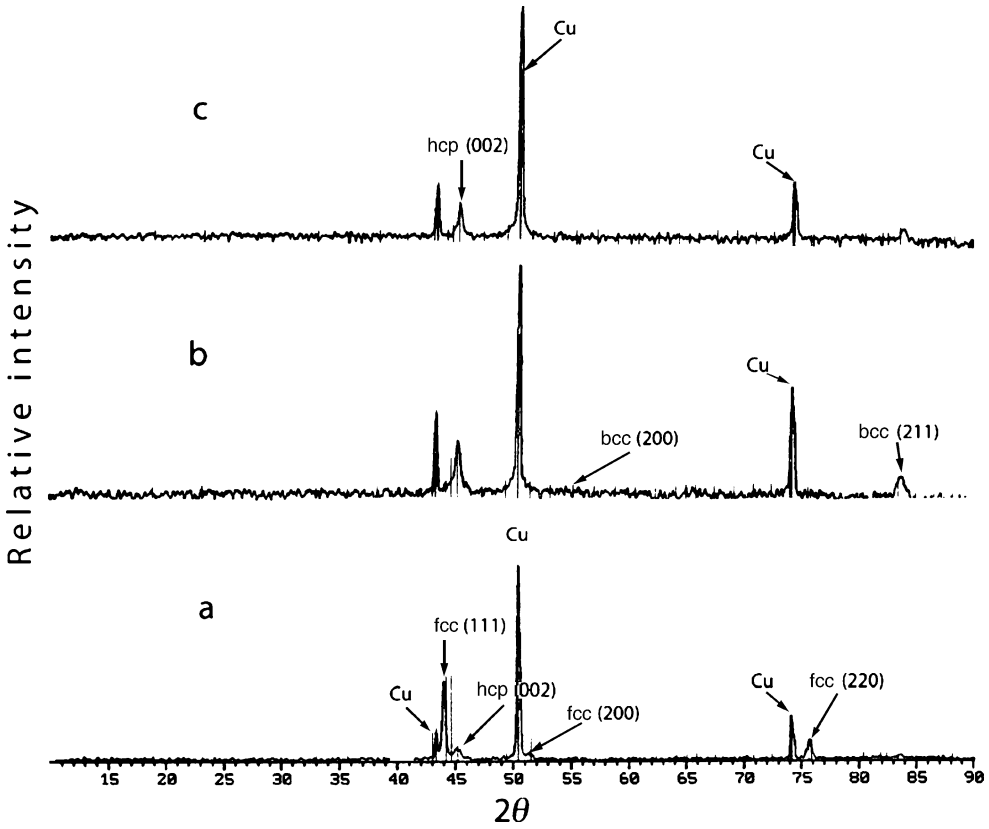

Fig. 5 X-ray diffraction patterns of as-deposited (i=13 mA/cm^2, t=200 s) thin film CoFeP alloy on Cu substrate with varying amounts of P as NaH_2PO_2. **a** 0 g/l NaH_2PO_2, **b** 1.0 g/l NaH_2PO_2, **c** 10.0 g/l NaH_2PO_2

formation, the lattice constant obtained for the FeCo (without P) alloy was 0.3472 nm. As the phosphorus content of the alloy increases, we observe that the preferred orientation of the alloy changes as indicated in the XRD peaks. The lattice constant for the CoFeP alloy was 0.2835 nm. This suggests the microstructure of the film changes with the presence of phosphorus as was observed from the AFM results. The addition of phosphorus into electrodeposited CoFe thin film produces nanocrystalline films whose crystal structure is modified. The modified crystal structure is expected in turn to affect the energy barriers required for the magnetic alignment of the grains. The crystalline films obtained for the as-deposited phosphorus containing CoFe alloy samples in this work contrasts with the results in [7, 8, 29] for which amorphous CoFeP deposits were obtained. Unlike the above referenced works in which the thin films contain high amount of phosphorus (>9 at.%) and produced the amorphous thin film, the deposits in the present work are nanocrystalline and contain less than 4 at.% P. EDS analysis was performed on the films to obtain their composition.

Table 2 illustrates a typical composition obtained at a current density of 10 mA/cm^2. Results in Table 2 suggest that when phosphorus-containing species is added to a CoFe alloy bath, co-deposition of phosphorus occurs at the expense of Co in the resulting alloy. The composition of the alloy shows an increase in phosphorus and Fe content whereas Co decreased. This change in alloy composition is reflected in the physical properties of the resulting film. As previously suggested, the differences in the microstructural features observed for the samples (e.g. Fig. 4a–c) are probably due to the presence of phosphorus in the films. At any operating current density, the co-deposited phosphorus in CoFe alloy film is dependent on the concentration level of phosphorus in the plating bath, pH and mass transfer effects.

Magnetic properties

The parameters extracted from hysteresis loop are often used to characterize magnetic properties of a magnetic thin film. Such magnetic properties include the magnetic saturation (M_s), the remanence (M_r), the squareness ratio or squareness (SQR or M_r/M_s) and the coercivity (H_c). Although some of these are intrinsic magnetic properties (e.g. M_s), the influence of preparation conditions of the thin film does influence the microstructure features on which

Table 2 Typical composition of CoFeP alloy deposited at a constant current density of 10 mA/cm^2

Elemental species	Sample A (at. wt.%)	Sample B (at. wt. %)	Sample C (at. wt. %)
Cobalt	80.71	75.7	74.2
Iron	19.29	22.7	22.5
Phosphorus	0	1.6	3.3

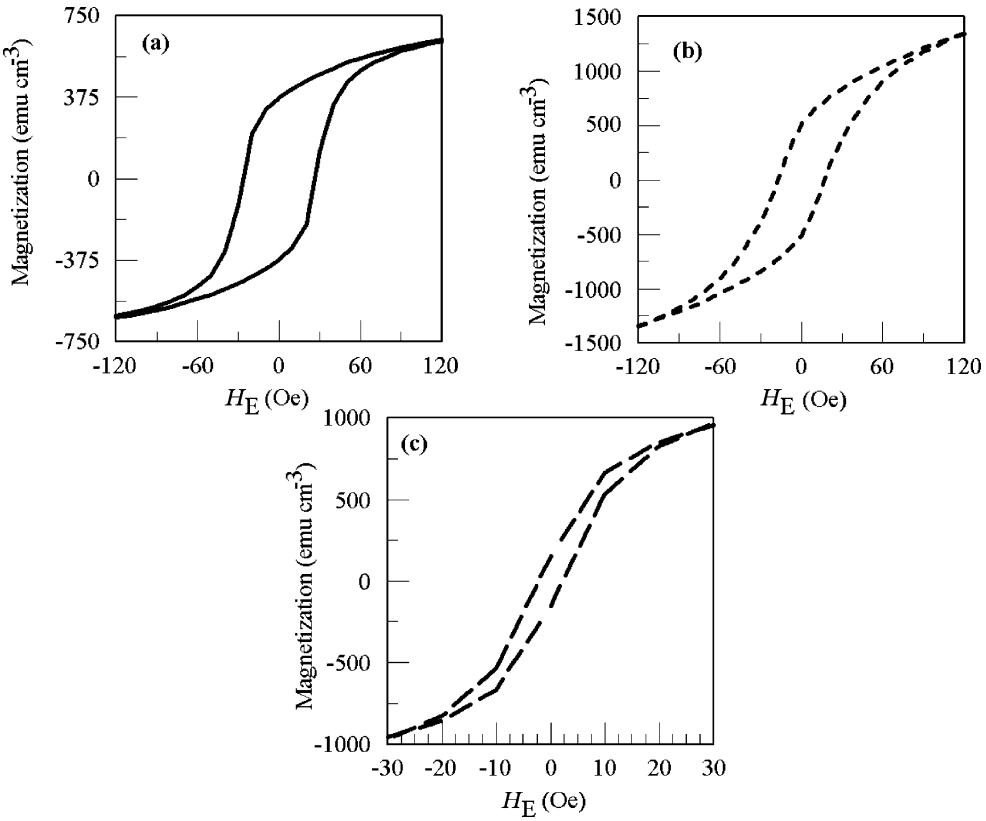

Fig. 6 Hysteresis loops of as-deposited CoFeP alloy films obtained from a SQUID magnetometer at 300 K. H_E was applied parallel to the film surface. **a** $Co_{80}Fe_{20}$, **b** $Co_{74}Fe_{23}P_3$, **c** $Co_{71}Fe_{23}P_6$

some of the properties depend. Figure 6 shows the hysteresis loops obtained for three films with differing amounts of phosphorus. The figure shows that increase in the amount of phosphorus in the CoFeP alloy leads to a narrower hysteresis loop that is less square than that obtained from CoFe alloy. The relationship between the NaH_2PO_2 concentration in the bath and the P content of the alloy is shown in Fig. 7a. It is observed that the P content of the alloy increased with increase in NaH_2PO_2 concentration. Within the narrow range of the deposit P content

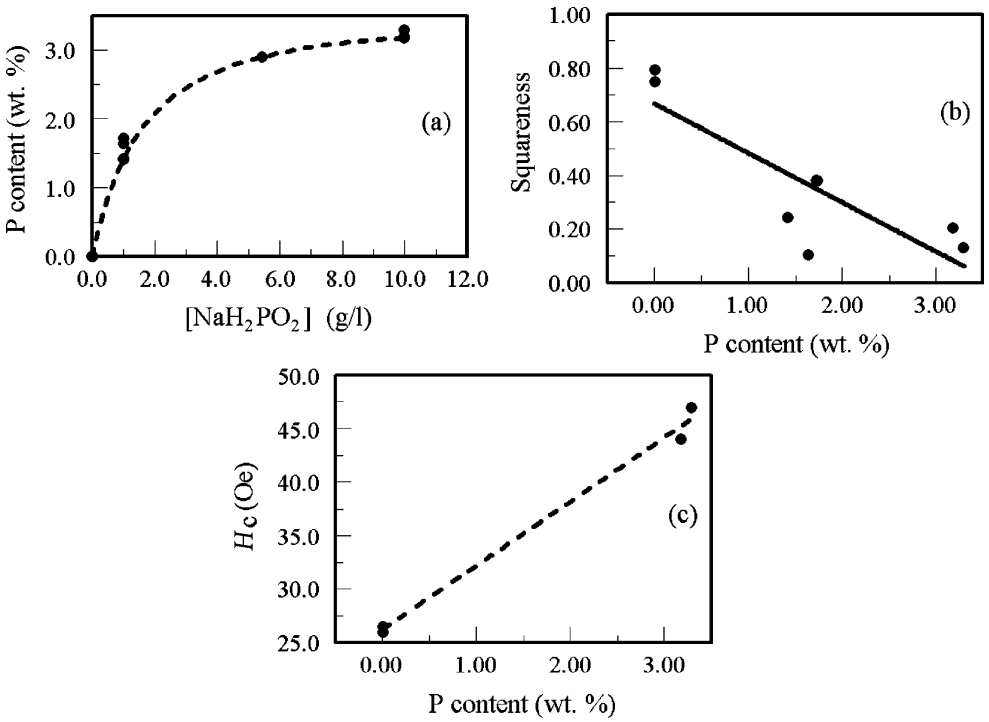

Fig. 7 Bath operating condition effects. **a** Dependence of P alloy content on the NaH_2PO_2 bath concentration. **b** Alloy P content effect on SQR or M_r/M_s. **c** Alloy P content effect on coercivity (H_c)

examined, the P content increases with NaH_2PO_2 concentration and tends to a limiting value. The SQR (parallel), a measure of how square the hysteresis loop is, is examined in Fig. 7b as a function of the P content of the thin film. As earlier shown, the amount of co-deposited phosphorus in the thin film is dependent on the concentration of phosphorus in the bath. Thus, the amount of phosphorus in the bath indirectly captures the microstructure effects on the magnetic property. The figure shows that within the experimental range of the present work, the SQR of the deposit decreases with increase in P content of the alloy or amount of P in the bath. This is in agreement with the results reported in reference [14] for CoNiP. Unlike the results obtained for CoNiP in reference [14], for the present work, we did not examine the limit of NaH_2PO_2 concentration at which the SQR does not change with increase in NaH_2PO_2. Further, whereas the current density was kept constant at 10 mA/cm^2 in reference [14], the present results were obtained at several different applied currents. We observe that SQR tends to decrease as bulk concentration of phosphorus in the bath increases as well as the current density. The relationship between SQR and the operating variables is probably due to the combined effects of phosphorus enrichment and film thickness.

Figure 7c shows the effect of phosphorus bath concentration on the film parallel coercivity, H_c. The H_c of the thin film, a complicated parameter, relates to the magnetic microstructure that involves a complex interplay of the effects of shape and dimensions of crystallites and nature of their boundaries etc. For the limited ranges of both parameters examined in Fig. 7c, low H_c values are obtained at lower P content in the alloy. Generally, H_c does not show a very strong dependence on the phosphorus content of the bath. This should be expected, as the amount of phosphorus considered in this work is very low.

Conclusion

Electrodeposited CoFeP thin films were studied using AFM, EDS, XRD and SQUID magnetometer techniques. The functional properties of electrodeposited CoFeP thin film depend on the microstructure and the evolution of the microstructural features is in turn dependent on the deposition conditions. The presence of low amount of phosphorus in the CoFe alloy changes its magnetic properties. The addition of phosphorus in CoFe alloy affects both its saturation magnetization and remanence and hence the SQR. The atomic percent P co-deposited with CoFe alloy depends on the concentration of phosphorus source in the plating bath. The presence of P in the CoFe alloy reduces the roughness of the deposit. The XRD studies show that crystalline CoFeP alloy deposits are obtained at low atomic percent P composition (<4 at.%), and the presence of P in CoFe changes its preferred orientation from fcc (111) plane to bcc (110) or hcp (002) plane.

Anomalous deposition of CoFe is explained as due to a change in the mechanism of the more noble species in the presence of the less noble component. The mechanism suggested differs from the previous mechanisms in the literature in that anomalous co-deposition does not involve the hydrated ions of the more noble species. Qualitative analysis suggests that CoFeP deposition is also anomalous. CoFeP thin film appears to have magnetic properties suitable for magnetic recording. Further examination of its corrosion resistance properties and quantitative analysis of its anomalous behavior are required.

Acknowledgments We thank Materials Research and Technology Center (MARTECH) at Florida State University for financial and analytical support. We would also like to acknowledge Dr. Eric Lochner for technical assistance with AFM and SQUID measurements.

References

1. Liao SH (1985) IEEE Trans Magn MAG-23:2981
2. Liao SH (1990) IEEE Trans Magn MAG-26:326
3. Ohshima N, Saito M, Ohashi K, Yamamoto H, Mibu K (2001) IEEE Trans Magn 37:1767
4. Chang JW, Andricacos PC, Petek B, Romankiw LT (1992) Proc 2nd Int Conf Magn Mater Processes Devices PV92-10:255
5. Liao SH, Roberts G, Darr E (1992) Dig Intermag Conf GC04:348
6. Omata Y, Kaminaka N (1992) Proc 2nd Int Conf Magn Mater Processes Devices PV92-10:255
7. Takai M, Nakamura A, Shigemoto R, Asa F, Osaka T (1995) Proc 4th Int Conf Magn Mater Processes Devices PV95-18:552
8. Hironaka K, Uedaira S (1990) IEEE Trans Magn 26:2421
9. Gigandet MP, Perrin FX, Pagetti J, Poupon G (2000) Mater Corros 51:418
10. Kim D, Park D-Y, Yoo B-Y, Sumodjo PTA, Myung NV (2003) Electrochim Acta 48:819
11. Kalu EE (1999) Proc 5th Int Symp Magn Mater Processes Devices PV98-20:545
12. Bertazzoli R, Pletcher D (1993) Electrochim Acta 38:651
13. Lallemand F, Ricq L, Wery M, Berqot R, Pagetti J (2004) Surf Coat Technol 179:314
14. Park D-Y, Myung NV, Schwartz M, Nobe K (2002) Electrochim Acta 47:2893
15. Myung NV, Park D-Y, Yoo B-Y, Sumodjo PTA (2003) J Magn Magn Mater 265:189
16. Garcia-Arribas A, Fdez-Gubieda ML, Orúe I, Barandiarán JM, Herreros J, Plazaola F (1995) Phys Rev B 52:12805
17. Kamei K, Maehara Y (1994) Mater Sci Eng A181/A182:906
18. Kakuno EM, Mosca DH, Mazzaro I, Mattoso N, Screiner WH, Gomes MAB, Cantão MP (1997) J Electrochem Soc 144:3222
19. Jay JP, Jêdryka E, Wojcik M, Dekoster J, Langouche G, Panissod P (1996) Z Phys B 101:329
20. Wojcik M, Jay JP, Panissod P, Jêdryka E, Dekoster J, Langouche G (1997) Z Phys B103:5
21. Jaya S, Rao ST, Rao GP (1985) Electrochim Acta 32:1053
22. Bockris JO'M, Drazic D, Despic AR (1961) Electrochim Acta 4:325

23. Zech N, Podlaha EJ, Landolt D (1999) J Electrochem Soc 146:2886
24. Zech N, Podlaha EJ, Landolt D (1999) J Electrochem Soc 146:2892
25. Hessami S, Tobias CW (1989) J Electrochem Soc 136:3611
26. Matlosz M (1993) J Electrochem Soc 140:2272
27. Bard AJ, Faulkner LR (1980) Electrochemical methods: fundamentals and applications. Wiley, New York, p 51
28. Kubaschewski O (1982) Iron binary phase diagrams. Springer, Berlin Heidelberg New York, p 27
29. Fukunaka Y, Aikawa S, Asaki Z (1994) J Electrochem Soc 141:1783